Journal of Controlled Release 363 (2023) 550–561

Contents lists available at ScienceDirect

Journal of Controlled Release

journal homepage: www.elsevier.com/locate/jconrel

A facile, flexible, and multifunctional thermo-chemotherapy system for customized treatment of drug-resistant breast cancer

Lili Chen [a], Ahmed Nabil [a,d], Nanami Fujisawa [a,d], Emiho Oe [a,d], Kai Li [a,b,e], Mitsuhiro Ebara [a,b,c,*]

[a] Research Center for Macromolecules and Biomaterials, National Institute for Materials Science (NIMS), 1-1 Namiki, Tsukuba, Ibaraki 305-0044, Japan
[b] Graduate School of Pure and Applied Sciences, University of Tsukuba, Tsukuba, Ibaraki 305-0006, Japan
[c] Department of Materials Science and Technology, Tokyo University of Science, Tokyo 125-8585, Japan
[d] Biotechnology and Life Sciences Department, Faculty of Postgraduate Studies for Advanced Sciences (PSAS), Beni-Suef University, Beni-Suef 62511, Egypt
[e] Ph.D. Program in Humanics, School of Integrative and Global Majors, University of Tsukuba, Tsukuba, Ibaraki 305-8575, Japan

ARTICLE INFO

Keywords:
Multidrug resistance
Hyperthermia
Thermo-chemotherapy
Nanofiber
Magnetic nanoparticles

ABSTRACT

Anticancer drug resistance invariably emerges and poses a significant barrier to curative therapy for various breast cancers. This results in a lack of satisfactory therapeutic medicine for cancer treatment. Herein, a universal vector system for drug-resistance breast cancer was designed to meet the needs of reversed multidrug resistance, thermo-chemotherapy, and long-term drug release behavior. The vector system comprises polycaprolactone (PCL) nanofiber mesh and magnetic nanoparticles (MNPs). PCL has excellent biocompatibility and electrospinning performance. In this study, MNPs were tailored to be thermogenic in response to an alternating magnetic field (AMF). PCL nanofiber can deliver various chemotherapy drugs, and suitable MNPs encapsulated in the nanofiber can generate hyperthermia and synergistic effect with those chemotherapy drugs. Therefore, a more personalized treatment system can be developed for different breast malignancies. In addition, the PCL nanofiber mesh (NFM) enables sustained release of the drugs for up two months, avoiding the burden on patients caused by repeated administration. Through model drugs doxorubicin (DOX) and chemosensitizers curcumin (CUR), we systematically verified the therapeutic effect of DOX-resistance breast cancer and inhibition of tumor generation *in vivo*. These findings represent a multifaceted platform of importance for validating strategic reversed MDR in pursuit of promoted thermo-chemotherapeutic outcomes. More importantly, the low cost and excellent safety and efficacy of this nanofiber mesh demonstrate that this can be customized multi-function vector system may be a promising candidate for refractory cancer therapy in clinical.

1. Introduction

Breast cancer is one of the most common types of malignant tumors among women [1]. Nevertheless, chemotherapy-the most commonly prescribed treatment in clinical practice-is less effective than expected, primarily because its effectiveness is impeded by multidrug resistance (MDR). Moreover, recent research has shown that MDR might facilitate tumor recurrence [2] and metastasis [3]. Thus, reverse MDR will be a crucial step in the fight against refractory breast cancer. Doxorubicin (DOX) is a highly effective drug for breast cancer treatment in the clinic, causing cell death through DNA insertion and the inhibition of topoisomerase II [4]. However, MDR through the P-glycoprotein (P-g protein), *etc.* pathway seriously impedes its clinical application [5,6]. It is worth noting that curcumin (CUR) is a low-toxicity natural drug derived from polyphenols in the Zingiberaceae plant family [7]. CUR, as a very effective P-g protein inhibitor, can reverse MDR and make MCF-7/ADR cells (human drug-resistant breast cancer) more sensitive to DOX [8]. However, CUR may not have effective *in vivo* effects since it may be difficult to accumulate in tumor cells and enter the same cancer cells as DOX.

A smart polymeric nanofiber structure has distinct advantages since its nano-scale features provide an enormous surface area and porous structure [9], enhancing its responsiveness to external stimuli, while its macroscale structures enable it to be easily manipulated in a bulk form

* Corresponding authors at: Research Center for Macromolecules and Biomaterials, National Institute for Materials Science (NIMS), 1-1 Namiki, Tsukuba, Ibaraki 305-0044, Japan.
E-mail address: EBARA.Mitsuhiro@nims.go.jp (M. Ebara).

https://doi.org/10.1016/j.jconrel.2023.10.010
Received 27 June 2023; Received in revised form 2 October 2023; Accepted 4 October 2023
Available online 9 October 2023

[10]. It is worth noting that polymer nanofibers can be mass-produced at low cost due to the low price of the polymer and the ease of manipulation of the nanofibers [11]. Magnetic nanofibers are based on a mild treatment strategy that exposes tumor tissue to higher temperatures than normal under a controlled magnetic field environment without causing any damage to normal tissue during treatment [12,13], has been developed in recent decades as an effective treatment system for deeply existing or localized cancers [14,15]. Furthermore, mild hyperthermia has also been used combined with chemotherapy to temporarily improve cancer cells' sensitivity to the damaging effects of chemotherapy drugs [16,17]. Nevertheless, the simultaneous encapsulation of magnetic nanoparticles and multiple drugs with unique physicochemical properties into a single nanosystem formulation remains challenging.

In this study, we attempted to design a flexible and multifaceted platform using polycaprolactone (PCL), a biodegradable material approved for biomedical applications by the U.S. Food and Drug Administration (FDA) [18]. Herein, PCL was used to fabricate a fiber mesh of nanoscale diameter through an electrospinning technique to entrapment of magnetic nanoparticles (MNPs) and load the chemotherapeutic drugs DOX and CUR (Scheme 1). Once the nanofiber mesh is transplanted into the tumor site, DOX and CUR could undergo sustained release by diffusion for more than two months from nanofibers. In addition, the nanofibers do not need to be harvested after treatment because they are biodegradable. Notably, CUR, as a chemosensitizer, suppresses DOX efflux and facilitates the intracellular accumulation of DOX in MCF-7/ADR cells by activating P-g protein down-regulation [19]. Consequently, CUR substantially reversed MDR and enhanced the cytotoxicity of DOX against MCF-7/ADR cells. Interestingly, MNPs play a crucial role in magnetic hyperthermia because they generate heat when exposed to an alternating magnetic field (AMF), which leads to cell death, and promotes chemotherapeutic efficacy [20]. Using a tumor-bearing nude mice model, we demonstrated that this nanofiber mesh showed an *in vivo* synergistic anticancer effect. Therefore, this readily processed multifaceted system could be an appreciable delivery vehicle for effective reverse MDR combined with thermo-chemotherapy. This custom combination therapy system is essential for validating this strategy to promote chemotherapeutic outcomes for the refractory tumor.

2. Materials and methods

2.1. Materials

Materials: Poly(ε-caprolactone) (Mw = 80 kDa), DOX (doxorubicin), and CUR (curcumin) were produced by Tokyo Chemical Industry Co., Ltd. (Tokyo, Japan). The nanopowder of iron (III) oxide (<50 nm particle size) was purchased from Sigma-Aldrich (Tokyo, Japan). The FBS (fetal bovine serum) was purchased from Tocris Bioscience Inc. (Minneapolis, MN, USA). RPMI 1640, MEM (modified Eagle's Medium), trypsin, penicillin, and streptomycin were bought from Nacalai Tesque, Inc. (Kyoto, Japan). MDA-MB-231 and MCF-7 cells (Human breast cancer cell lines) were provided by the American Type Culture Collection (Manassas, VA, USA). The human breast cancer adriamycin-resistant cell line MCF-7/ADR was obtained from Icell Biscience Inc. (Shanghai, China). Charles River Laboratories Japan, Inc. provided the female BALB/C nude mice (Yokohama, Japan).

2.2. Fabrication and characterization of nanofiber mesh

We fabricated PCL nanofiber meshes following a previously published procedure [21]. The electrospinning solution was prepared by dissolving PCL in HFIP at 20% (*w/v*). A PCL solution was prepared by mixing MNPs, CUR, and DOX at 30% (w/v), 0.22%, and 0.46% (*w/w*), respectively. The nanofibers were produced through an electrospinning system (Nanon-01 A, MECC Co., Ltd., Fukuoka, Japan). The liquid

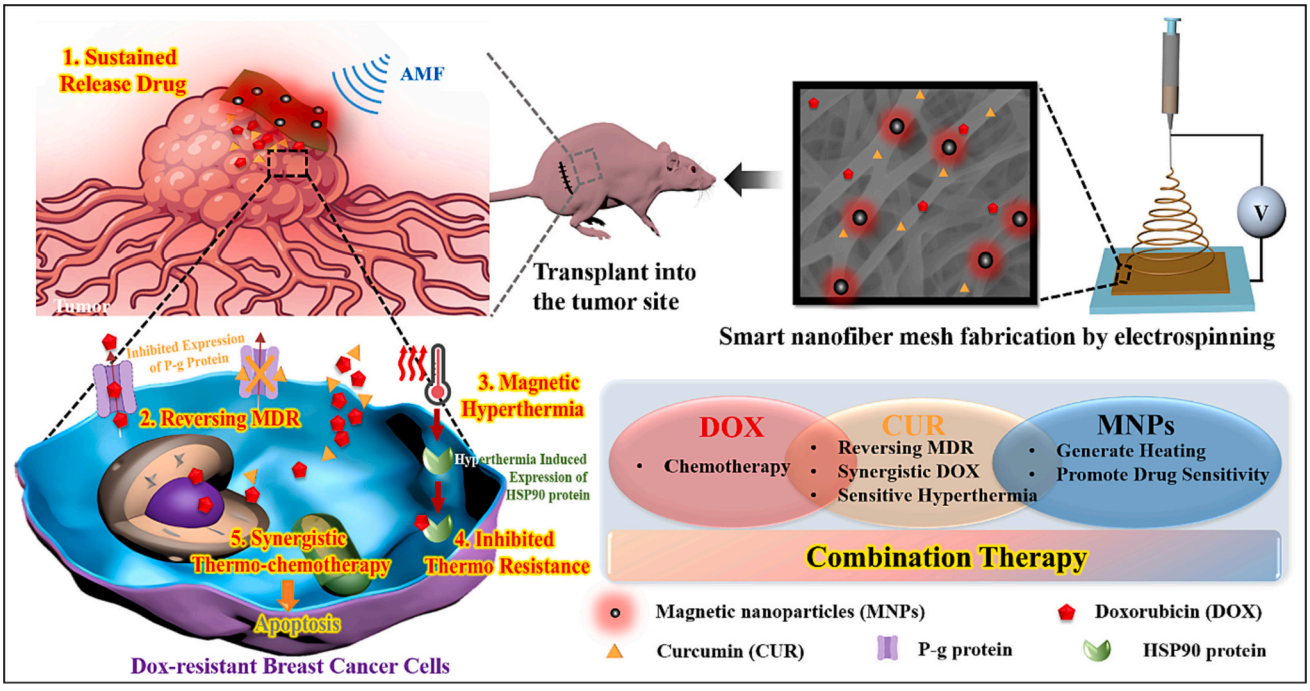

Scheme 1. Schematic diagram to illustrate the manufacture of multifunctional nanofiber mesh capable of simultaneously delivering magnetic nanoparticles and chemotherapeutic drugs (DOX and CUR) for synergistic inhibition of intractable drug-resistant breast cancer therapy: a). The MNPs-loaded nanofiber can provide controlled heating with an external AMF to achieve thermotherapy and increase cell sensitivity to drugs. b). The sustained release of DOX and CUR over two months provides long-term antitumor activity. The intelligent nanofiber mesh encapsulates the P-glycoprotein interference drug CUR to reverse MDR by inhibiting DOX efflux by tumor cells. c). CUR also improves the hyperthermia effect by interfering with the expression of the thermo-resistance protein (HSP90 protein). A multipronged thermo-chemotherapy strategy involving nanofibers can provide mutual enhancement by reversing MDR and promoting drug sensitivity through hyperthermia.

surface tension was overcome by applying a voltage of 20 kV to the polymer solution and forming a polymer jet. The nanofibers were collected from the syringe needle on an eight cm collector plate. The experiment was conducted at room temperature with a flow rate of 1.0 mL/h. After Pt coating, nanofiber morphologies were observed using scanning electron microscopy (SEM, SU8000, Hitachi High-Technologies Corporation, Tokyo, Japan). Nanofiber diameters were determined using ImageJ and the diameter J plugin. For localizing the MNPs within the fibers, EDX-SEM mapping (FE-SEM SU8000 EDX, Hitachi High-Technologies Corporation, Tokyo, Japan) was performed (with Bruker QUANTAX EDS for SEM, 5 kV).

2.3. Heating profiles for nanofiber mesh

Nanofiber meshes with MNPs (40 mg) were investigated under AMF irradiation to evaluate their heat-generating properties. We used a customized copper coil to incorporate the nanofiber mesh and the mesh was exposed to HOTSHOT 2 (Alonics Co., Ltd., Tokyo, Japan)to generate an AMF (480 A, amplitude 281 kHz frequency). Temperature changes in the nanofiber mesh were recorded at a predetermined interval using a FLIR thermo-camera (CPA-E6, FLIR Systems Japan K.K., Tokyo, Japan).

2.4. In vitro drug release

An investigation of the drug release behavior of nanofibers was conducted in phosphate-buffered saline (PBS) solution. The nanofiber meshes (40 mg) were immersed in 5 mL of PBS solution for 60 days while being shaken at 37 °C. AMF was applied every three days for 15 min. We deducted and replaced 3 mL of PBS at predetermined intervals. Following that, fluorescence measurements for DOX (excitation 485 nm, emission 595 nm) and absorbance measurements for CUR (345 nm) were performed using a plate reader (Infinite 200PRO, Switzerland). DOX and CUR loading and release from nanofibers were further investigated using confocal laser scanning microscopy (CLSM), and images were captured and analyzed using ZEN 2010 software. Drug fluorescence was detected at different release times from nanofibers. The fluorescence of DOX and CUR (DOX, 485 nm excitation, 595 nm emission; CUR, 342 nm excitation, 475 nm emission) were obtained on a CLSM (Zeiss LSM 700, Japan).

2.5. The cellular uptake of drugs

The cellular uptake behavior of release DOX from nanofiber mesh was investigated by fluorescence microscopy in MCF-7/ADR cells. Briefly, the cells were seeded onto 6-well plates at a 1.0×10^5 cells/well density. After 24 h, the cells were further incubated with nanofiber mesh for another 48 h. PBS was used to wash the cells, and exclusive nuclear dye DAPI (Sigma-Aldrich, USA) was used to stain the cells for 30 min. The fluorescence images of cells were obtained using an OLYMPUS IX71 fluorescence microscope.

2.6. Evaluation of combination efficacy of drugs and hyperthermia

The breast cancer cells were cultured in MEM or RPMI 1640 media. A density of 1.0×10^4 cells was plated in 96-well plates, and the cells were cultured for 24 h. To investigate the combined efficacy of CUR and DOX, the cells were replenished with fresh medium supplemented with 6.21 μg/mL of CUR (around IC_{30}) and DOX at the appropriate concentration. For evaluating the efficacy of drugs enhanced by hyperthermia, fresh medium was replaced by heating to 43 °C and supplemented with DOX or CUR at the appropriate concentration. Cells were incubated for an additional 48 h at 37 °C after being incubated at 43 °C. Afterward, MTT was used to determine the viability of the cells. Drug resistance index (DRI) and reversal index (RI) were calculated as follows: $DRI=IC_{50\ cells\ 1}/IC_{50\ cells\ 2}$, $RI=DRI_{DOX}/DRI_{DOX\ +\ CUR}$ [19].

2.7. Cell scratch assay

Cell scratch assays were conducted to examine the inhibitory efficacy of the proposed nanofiber mesh on tumor cell growth. MCF-7/ADR cells were plated in six wells. A sterile 200 L pipette was used to scrape off the monolayer cells attached to the wall, and gentle washing with PBS was performed on the scraped cells. An AMF was applied to the nanofiber mesh (40 mg weight) for 15 min, and the mesh was then cultured in an incubator for 48 h. The migration profiles of tumors cell were observed in an inverted microscope and photographed. The relative migration of cells was calculated using the formula: Relative migration = $(Width_{0\ h} - Width_{24\ h})/Width_{0\ h}$.

2.8. Antitumor efficacy of the nanofiber mesh

For the synergistic anticancer experiment, 10^6 cells of MCF-7/ADR were plated per dish in a 35 mm dish for 24 h. The nanofiber mesh was immersed into the medium after being sterilized by ethylene oxide gas (EOG). The nanofibers were suspended in the medium and exposed to AMF for 15 min. Following incubation at 37 °C for 48 h, the cell number was determined using the MTT assay.

2.9. Apoptosis assay

An investigation of apoptosis in MCF-7/ADR cells treated with nanofiber mesh was conducted using Annexin V-FITC/PI flow cytometry. The nanofiber mesh was co-incubated with cells exposed to AMF for 15 min and cultured for 48 h at 37 °C. Additionally, MCF-7/ADR cells were washed with pre-cooled PBS, trypsinized, collected, and re-suspended in 200 mL binding buffer before being analyzed. Subsequently, the above cell suspension was incubated in the dark for 15 min with Annexin V-FITC and PI. Staining was observed using flow cytometry, and untreated cells served as control.

2.10. Western blot assay

Proteins were extracted from a cell lysate containing protease inhibitors. The sample's concentration was determined by a Nanodrop™ 2000 analyzer (Thermo-Fisher Scientific, USA). SDS-PAGE was used for cell lysate separation, then transferred to PVDF membranes. Following three hours of blocking with 5% skim milk at 37 °C, the membranes were incubated with primary antibodies against P-g and HSP90 proteins (P-g and HSP90 at 1:500 dilution, β-actin at 1:500 dilution, Abcam, US) overnight at 4 °C. Afterward, we washed and incubated the membranes for an hour at room temperature with the secondary antibody, HRP-labeled goat-anti-rabbit IgG, at 1:5000 dilution (Abcam, US). The immunoreactivity signal was assessed using an ECL Advance Western Blotting Detection Kit (Bioworld Technology) with β-actin as an internal control. LumiCube was used to analyze signals (Media Cybernetics, Rockville, MD).

2.11. Anti-tumor efficacy by nanofiber mesh

Female BALB/C nude mice aged 4–6 weeks were subcutaneously injected with MCF-7/ADR cells (10^8 cells/mL^{-1}) and randomly assigned to nine groups ($n = 7$). Nanofibers were implanted adjacent to the tumor region in mice once the tumor volume reached approximately 50 mm^3. The mice with nanofibers were subjected to AMF once a week for 15 min over three months. DOX and CUR were also administered directly into the tumor area of the mice (free drugs group). Calculate tumor volume (V) based on the formula $V = 0.5 \times a \times b^2$, where a and b represent the major and minor axes of the tumor, respectively. Blood samples were collected from the heart to determine levels of alanine aminotransferase (ALT) and glutamic oxaloacetic transaminase (AST) through an ELISA. The Experimental Animal Administration Committee of the National Institute for Materials Science experimental procedures and all

approved animal care.

2.12. H&E assay and immunohistochemical analysis

For histological analysis, sacrificed nude mice's major organs and tumors were fixed overnight in 4% paraformaldehyde. The paraffin-embedded specimens were cut into 5 mm thick sections and successfully dewaxed and rehydrated in xylene, ethanol, and deionized water. Lastly, H&E staining was performed on the slides to assess the histological alterations under a microscope.

Following with the previous description, paraffin-embedded tumor sections were prepared and processed for immunohistochemical analysis [22,23]. The expression of P-g protein and HSP90 protein in the sections was examined with monoclonal antibodies to P-g and HSP90 at 1:100 dilutions. Reddish-brown precipitation was observed in the cytoplasm of the positive reaction under a microscope.

2.13. Masson trichrome staining

Firstly, the slides were deparaffinized and hydrated with distilled water. Mordanted in Bouins's solution (Fisher Scientific, NC082706), stained slides were preheated to 58 °C for 15 min. After washing with distilled water, slides were stained in modified Weigert's iron hematoxylin, protected from light, and washed with distilled water. Differentiated the slides in acid-alcohol solution, Dietrich scarlet-acid fuchsin solution, 1% phosphomolybdic acid, and blue aniline solution. After the slides were washed, the acetic acid solution was dehydrated in graded alcohols and cleared in Xylene. Finally, Masson trichrome staining was performed to assess histological alterations with the microscope, and collagen fiber area percentage was determined using ImageJ software. The surface area percent occupied by fibrosis (blue area) was measured within the defined frame using the Image-J after color deconvolution. The proportion of fibrosis on an optical field was fibrosis area/reference

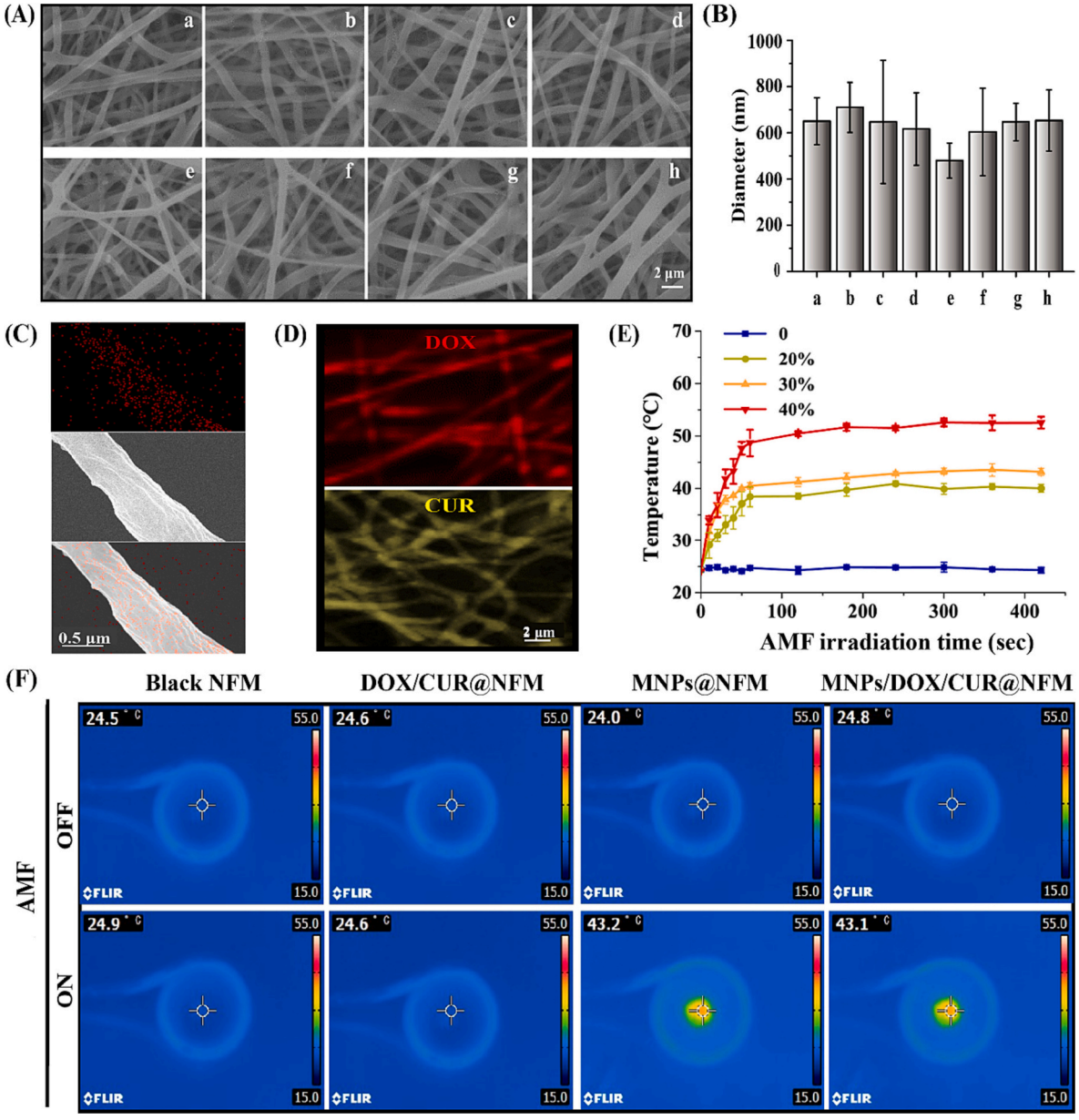

Fig. 1. (A) Image of nanofiber mesh obtained by SEM. (B) The average diameter of nanofibers. (a: Blank NFM, b: MNPs@NFM, c: DOX@NFM, d: CUR@NFM; e: MNPs/DOX@NFM; f: MNPs/CUR@NFM; g: DOX/CUR@NFM; h: MNPs/DOX/CUR@NFM) (C) Elemental mapping image of MNPs/DOX/CUR@NF mesh. (D) Confocal laser scanning microscope image of nanofiber meshes. (E) MNPs@NFM heating profiles during AMF at varying times for nanofiber meshes with different proportions of MNPs. (F) The Infrared thermal images of nanofiber meshes exposure AMF for 15 min.

area. The results were expressed as a mean of 5 ± SD.

2.14. Statistical analysis

All experiments were conducted in triplicate, and the data were expressed as mean ± standard deviation (SD). For statistical analysis, student's *t*-tests and one-way analysis of variance (ANOVA) were performed using Origin version 9.0 software (Northampton, USA). The difference between the results was considered statistically significant for $p < 0.01$ (**) and $p < 0.05$ (*).

3. Results and discussion

3.1. Fabrication of nanofiber meshes

Our previous work described the development of PCL electrospun nanofiber meshes incorporating a variety of therapeutic agents for cancer treatment [21,24]. In these studies, we found that PCL solution viscosity [25] and different molecular weights were essential to maintain PCL-based fiber morphology and crystallinity during AMF irradiation, which may impact sustained drug release. Given these caveats, electrospinning PCL nanofiber meshes under optimal conditions were employed to fabricate them.

Fig. 1 (A) shows SEM (scanning electron microscope) images of the nanofiber mesh containing CUR, DOX, and MNPs. There are no beads in the morphology of the nanofibers, which shows a uniform fiber diameter distribution. According to Fig. 1 (B), nanofibers have an average diameter of 500–700 nm, while MNPs/DOX/CUR nanofibers have a diameter of 653 ± 132 nm.

Fig. 1 (C) shows the EDX of the nanofiber mesh, demonstrating the homogenous distribution of MNPs (Fe elements) across the entire mesh without large aggregates. The uniform fluorescence distribution in Fig. 1 (D), shown in the confocal laser scanning microscope image, indicates that DOX and CUR are distributed evenly within the nanofibers. The homogeneous dispersion of MNPs and drugs within the nanofiber mesh is associated with constant hyperthermia and drug sustained release, making this observation essential.

3.2. MNPs heating profiles within nanofiber meshes

Hyperthermia caused by magnetic fields treats tumors by irradiating magnetic nanoparticles with AMF to generate heat. Due to AMF's high tissue penetration, it can precisely treat deep tumors [26,27]. Consequently, it is essential to analyze the heating potential of MNPs in nanofiber meshes exposed to AMF [28]. The MNPs in this study are Fe_2O_3 nanoparticles, and the saturation magnetization was 57 emu g^{-1}. Further, an AMF of 281 kHz was used in this study for suitable clinical applications (the frequency threshold for AMFs is 100–300 kHz) [29].

In Fig. 1 (F), the infrared thermal images show nanofiber mesh (12.0 mg MNPs) after 15 min of AMF irradiation. An AMF-exposed mesh of MNPs@NFM and MNPs/DOX/CUR@NFM reached 43.2 °C and 43.1 °C, respectively. According to Fig. S1 (A), the mesh with 20% MNPs only experienced minimal temperature changes within 15 min. Nevertheless, 30% and 40% of fiber meshes loading with MNPs showed significant changes.

In addition, we detected the temporal temperature changes in nanofiber meshes during AMF irradiation. Figs. 1 (E) and S1 (B) suggested that the heating rates of the MNPs loaded in the nanofiber meshes vary depending on the amount and time. Moreover, DOX and CUR did not significantly affect the heat-generation behavior of the nanofiber meshes with incorporated MNPs.

3.3. In vitro drug release behavior

Since nanoparticles have a limited loading capacity, the long-term release of drugs takes time and effort. [30]. Nanofiber meshes provide a superior capacity for drug loading and a more prolonged release potential due to their proprietary features compared to these nanoparticle drug-delivery platforms. MNPs/DOX/CUR nanofibers (with or without AMF) successfully sustained released DOX and CUR for 60 days in Fig. 2 (A). Additionally, at 60 days, over 30% of the loaded DOX and approximately 25% of the CUR contents were released from the nanofiber mesh when AMF was applied and unapplied. The difference between DOX and CUR release profiles could be caused by the different solubility of the two drugs in PBS. This leads to different drug release efficiencies, even though both drugs are evenly distributed within the nanofibers. Furthermore, there was no significant change in the profiles of DOX and CUR released from the nanofiber mesh with or without AMF, indicating that AMF irradiation did not affect the drug release behavior. In addition, as shown in Fig. 2 (B) confocal laser scanning microscope image, the fluorescence of the nanofibers after 48 h of release was significantly weaker than after 2 h, confirming that the fluorescent drugs CUR and DOX can be released from the nanofibers.

3.4. Analyses of cellular uptake and distribution of DOX

The intrinsic fluorescence of DOX was used as a model drug to analyze the cellular uptake and distribution of drugs released from a nanofiber mesh. Fig. 2 (C) shows that the fluorescent intensity in MNPs/DOX/CUR nanofiber mesh-treated cells was significantly more potent compared to blank nanofiber mesh and MNPs/DOX nanofiber mesh. It demonstrated the efficiency of CUR in taking up DOX into cells. It is might be because CUR acts as a chemosensitizer, resulting in the downregulation of the P-g protein in MCF-7/ADR cells, thus suppressing the efflux of DOX and facilitating its intracellular accumulation. It is also notable that DOX's red fluorescence is present in the nuclei of MCF-7/ADR cells, which can exert antimitotic effects. This result coincided with the high cytotoxicity of the MNPs/DOX/CUR nanofiber mesh. It emphasized the critical function of nanofiber sustained release and drug internalization in enhancing cytotoxic activity.

3.5. Cytotoxic potency of DOX markedly stimulated by CUR and hyperthermia

The viability of breast cancer cells was analyzed to reverse the effect of CUR on DOX. As indicated in Fig. 3 (A), the IC_{50} values of DOX for MCF-7, MDA-MAB-231 and MCF-7/ADR cells were measured to be 0.45 μg/mL, 0.90 μg/mL and 78.96 μg/mL, respectively. MCF-7/ADR cells have a significantly higher IC_{50} than MDA-MB-231 and MCF-7 cells, due to the DOX-resistant effect. However, the CUR IC_{50} against those three cells showed no significant difference in Fig. 3 (B). Furthermore, to evaluate the CUR reverse effects on multidrug-resistant breast cancer cells, the IC_{50} of DOX was evaluated by MCF-7 and MCF-7/ADR cells treated with varying concentrations of DOX combined with the IC_{30} concentration of CUR. In MCF-7/ADR cells, compared with the IC_{50} of DOX alone in Fig. 3 (A), the IC_{50} of DOX synergistic with CUR was significantly reduced from 78.96 μg/mL to 22.95 μg/mL in Fig. 3 (E). Even though the cytotoxicity of MCF-7 and MDA-MB-231 cells using DOX/CUR (Fig. 3 (E)) was slightly lower at higher DOX concentrations (2.5 μg/mL) than with DOX only (Fig. 3 (A)), it may be due to the protective effect of CUR, cellular response modulation, and metabolic interference. However, the DRI (the ratio of IC_{50} values between MCF-7/ADR and MCF-7 cells) of DOX was calculated as 175.47 (Table S1), indicating that MCF-7/ADR cells were highly resistant to DOX. The reversal index was calculated as the formula: $RI = DRI_{DOX}/DRI_{DOX + CUR}$. The reversal of DOX + CUR for MCF-7/ADR cells was 3.13 and 3.11-fold for MCF-7 and MDA-MB-231 cells, respectively, which meant CUR had strong suppression to MDR in MCF-7/ADR cells.

Hyperthermia induced by MNPs enhances the cytotoxicity of certain chemotherapeutic drugs, including DOX, curcumin, PTX, and salinomycin. It is because mild hyperthermia (43–45 °C) increases the permeability and spacing within tumor cells, increasing the tumor's

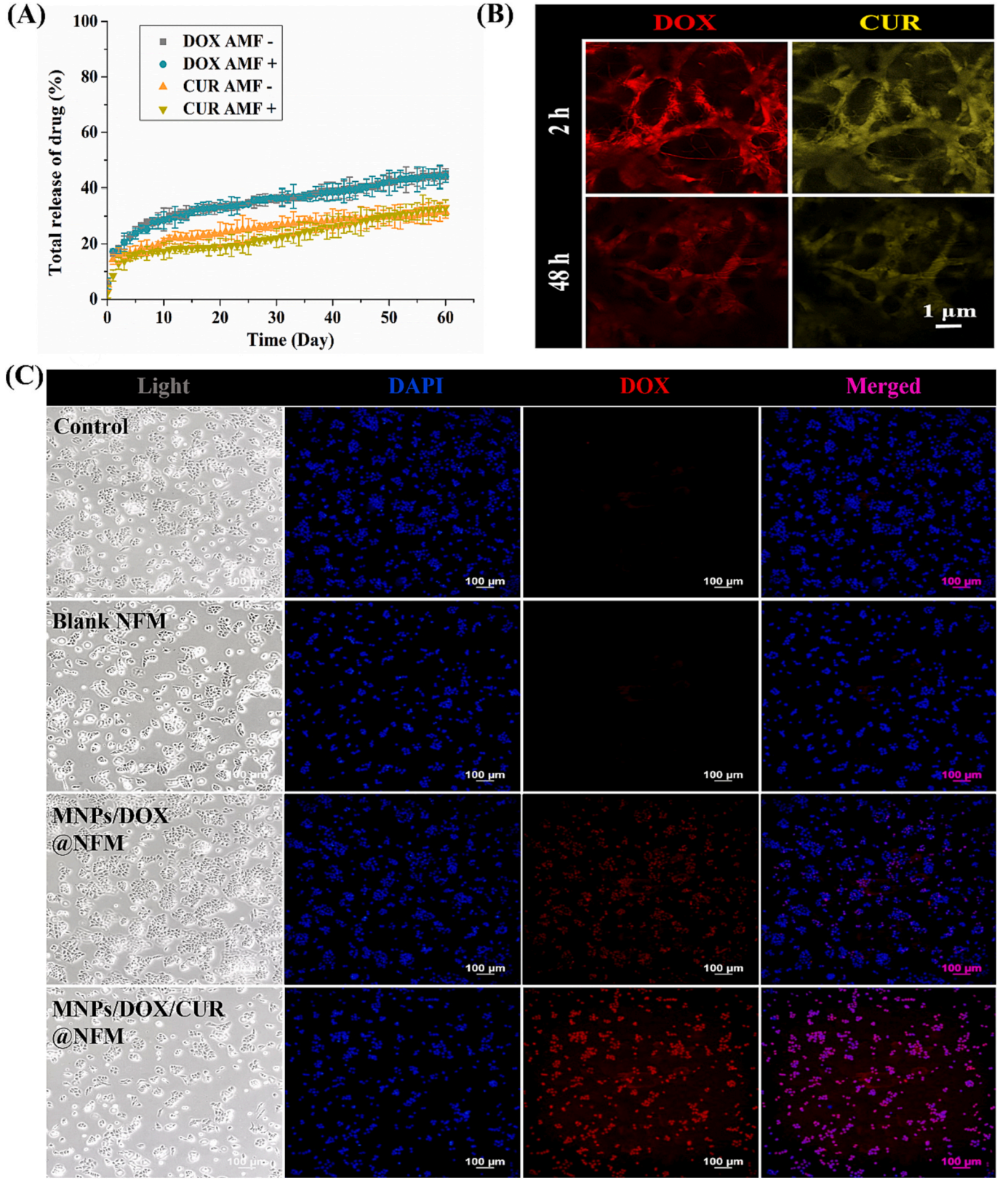

Fig. 2. (A) Release profiles of DOX and CUR from the MNPs/DOX/CUR nanofiber mesh with various nanofiber meshes with and without AMF; the nanofiber meshes were irradiated with AMF for 15 min every three days. (B) Confocal laser scanning microscope image of MNPs/DOX/CUR nanofiber mesh. (C) Cellular uptake and localization of DOX in MCF-7/ADR cells were observed by fluorescence microscopy after cells were incubated with the nanofiber mesh for 48 h.

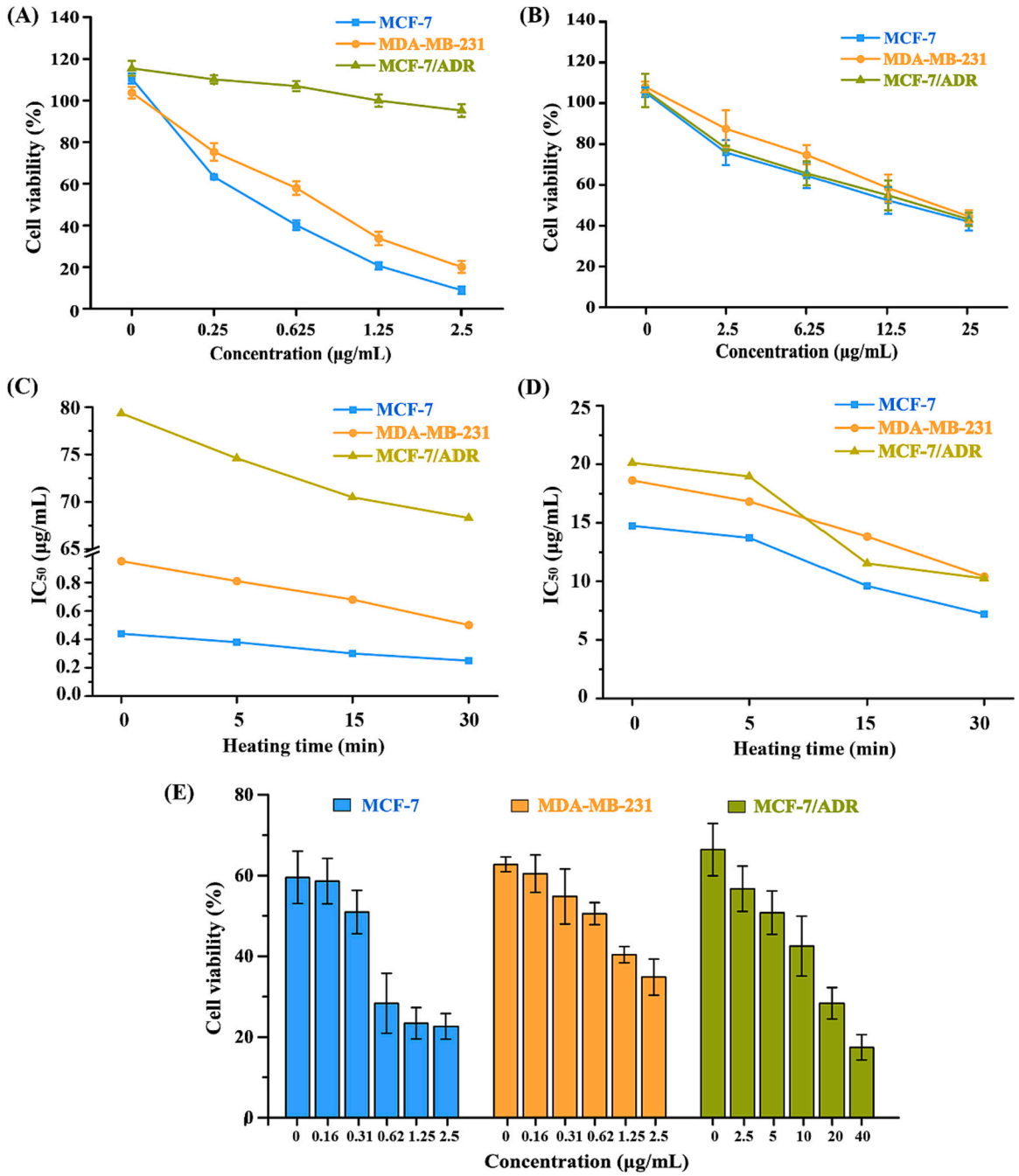

Fig. 3. Viability of MCF-7, MDA-MB-231, and MCF-7/ADR cells treated with different concentrations of (A) DOX and (B) CUR at 48 h; The changing of IC_{50} of (C) DOX and (D) CUR against MCF-7, MDA-MB-231, and MCF-7/ADR cells with different heating times (at 43 °C) at 48 h. (E) The cell viability of MCF-7, MDA-MB-231, and MCF-7/ADR cells treated with different concentrations of DOX combined with the same concentration of CUR (IC_{30}) at 48 h.

sensitivity to chemotherapy [31]. In order to evaluate the synergistic effects of hyperthermia and drugs (DOX and CUR) on breast cancer cells, the IC_{50} of drugs was evaluated by varying the heating time. IC_{50} values for DOX and CUR are significantly reduced with increasing heating time (Fig. 3 (C) and (D)). Interestingly, the effect of heating on MCF-7/ADR cells was also shown, with DOX IC_{50} dramatically dropping for longer heating times. A decrease in IC_{50} of DOX was detected from 79.4 μg/mL to 70.5 μg/mL compared to cells that were not heated. Furthermore, Fig. 3 (D) shows a decrease in the IC_{50} of CUR against breast cells, possibly due to a thermal denaturation effect on proteins and DNA of cells and enhanced permeability of cancerous cell membranes. Further, heating enhances the anticancer properties of the drug by crosslinking it with DNA and impairing the ability to repair damage caused by the drug [31]. It is particularly hypoxic tumor cells that are most sensitive to heat [32].

3.6. *Synergistic anticancer effects of nanofiber mesh*

The above experimental results demonstrated that this nanofiber mesh potentially applies to thermo-chemotherapy and reversed DOX resistance in DOX-resistant breast cancer cells. The MNPs/DOX/CUR nanofiber mesh was further investigated for synergistic antitumor effects on MCF-7/ADR cells. The apoptosis of MCF-7/ADR cells induced by nanofiber mesh was first examined using flow cytometry using a double stain of Annexin V-FITC and PI. As illustrated in Fig. 4 (A), only 10.8% and 52.3% of apoptotic and dead cells, respectively, were induced by

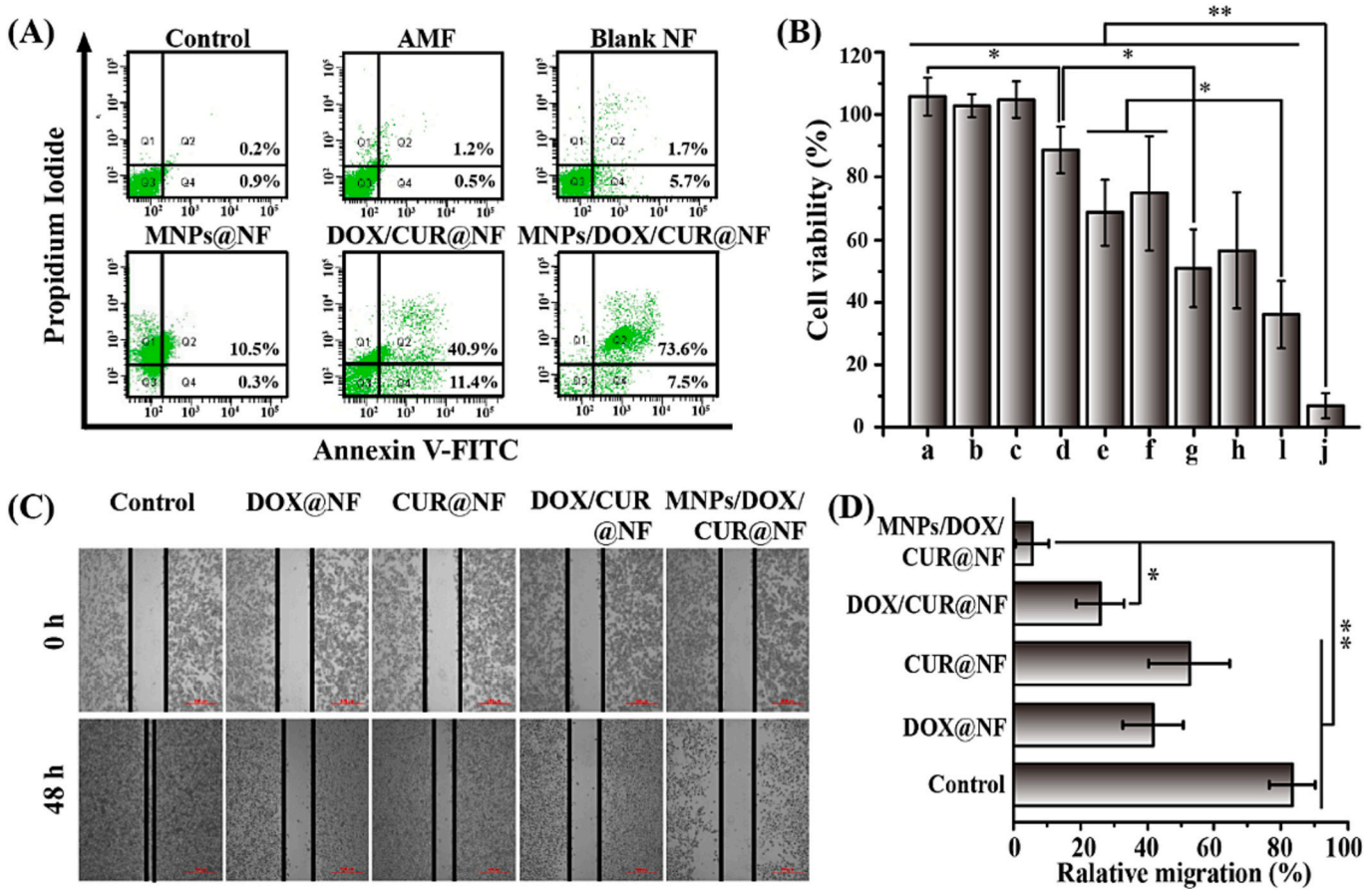

Fig. 4. *In vitro* antitumor effect of nanofiber mesh in 15 min AMF application on MCF-7/ADR cells by (A) apoptosis analysis, (B) MTT assay, and (C) scratch assays. (D) The quantified relative migration summarized as a bar graph. (Data are mean ± SD $n = 3$, $^{*}p < 0.05$, $^{**}p < 0.01$). (a: Control, b: Blank NFM, c: AMF, d: MNPs@NFM + AMF, e: DOX@NFM + AMF, f: CUR@NFM + AMF, g: MNPs/DOX@NFM + AMF, h: MNPs/CUR@NFM + AMF, i: DOX/CUR@NFM + AMF and j: MNPs/DOX/CUR@NFM + AMF).

hyperthermia (MNPs@NFM) and chemotherapy (DOX/CUR@NFM) groups. The exposure of MNPs to AMF induced a temperature increase to about 43 °C by generating magnetic heat, which caused the death of some tumor cells, suggesting that necrotic cell death also occurs with only hyperthermia. This result is consistent with the results of cytotoxicity experiments (Fig. 4 (B)). By contrast, thermo-chemotherapy induced a higher apoptosis rate (81.1%), which was remarkably higher than any other group. These findings suggested that the hyperthermia generated by MNPs/DOX/CUR nanofiber mesh exposed to AMF made cancer cells more sensitive to synergistic chemotherapy and thus efficiently induced cell apoptosis.

Additionally, MNPs/DOX/CUR nanofiber mesh was evaluated for its cytotoxicity using the MTT method to investigate its antitumor effect. As displayed in Fig. 4 (B), compared to the single drug-loaded groups (DOX@NFM and CUR@NFM), the cytotoxicity increased sharply in the DOX/CUR@NFM group, which is consistent with the results in Table S1. Moreover, MNPs/DOX/CUR@NFM emerged with significantly higher cytotoxicity than other treatments. It demonstrates that the MNPs/DOX/CUR nanofiber mesh could achieve synergistic anticancer efficiency by reversing DOX resistance and improving the anticancer effect of chemotherapy through hyperthermia.

Tumor metastasis is a major factor in breast cancer death [33]. Therefore, cell scratch assays were conducted to examine the nanofiber mesh to prevent the migration of MCF-7/ADR cells. Fig. 4 (C) shows that cells incubated with MNPs/DOX/CUR@NFM experienced a significant reduction in relative migration rate to only 5.6% compared to cells incubated with other groups, demonstrating the synergistic effects of hyperthermia and chemotherapy on the cell viability and migration of MCF-7/ADR cells, which ultimately resulted in a decrease in invading growth.

These results confirm that our thermo-chemotherapy system could synergize by hyperthermia and chemotherapy synergize in promoting cancer cell death and apoptosis, even degrading tumor aggressiveness, which sheds light on augmented anti-cancer chemotherapy.

3.7. *The mechanism for the enhanced anticancer activity of a nanofiber mesh*

To analyze the mechanism of the enhanced anticancer effect of the thermo-chemotherapy system (MNPs/DOX/CUR nanofiber mesh), we again treated MCF-7/ADR cells with nanofiber meshes. The expression of a drug-resistant related protein (P-glycoprotein, P-g protein) and thermo-resistant related (heat shock protein, HSP90) was evaluated using western blot. The P-g protein reduction for MCF-7/ADR cells under incubation with a CUR-containing nanofiber mesh was confirmed by western blot. In Fig. 5 (A), contrary to the substantial expression of P-g protein in the control groups, P-g protein was markedly reduced in cells incubated with MNPs/CUR@NFM, even in cells treated with MNPs/DOX/CUR@NFM. To this end, the functional roles of CUR were demonstrated for reversed DOX-resistance through P-g reduction; thus, the improvement of DOX on the chemotherapeutic efficacy in MCF-7/ADR cells.

Fig. 5 (B) indicates that MCF-7/ADR cells treated with MNPs@NFM expressed a significantly higher level of HSP90 ($p < 0.05$) than the control, which may be caused by the heating generated by the MNPs in nanofibers. However, the CUR@NFM groups showed a notable decrease

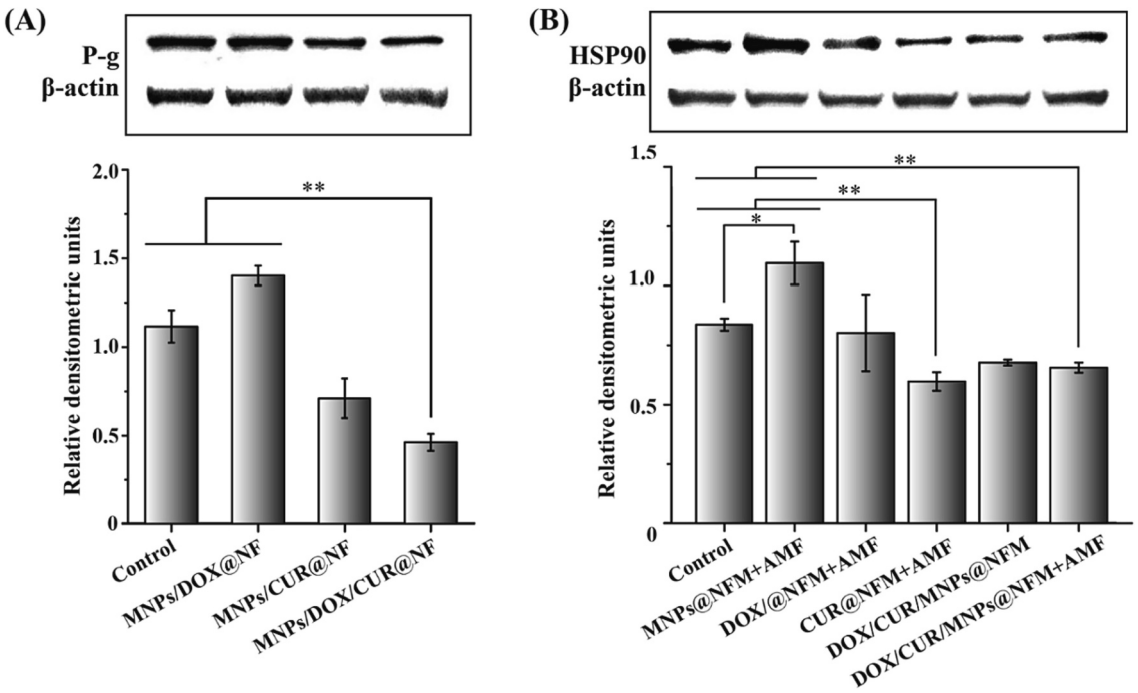

Fig. 5. Western blot analysis of (A) P-g protein and (B) HSP90 protein expression in MCF-7/ADR cells after different nanofiber mesh treatments. (Data are mean ± SD $n = 3$, $^{*}p < 0.05$, $^{**}p < 0.01$).

in HSP90 expression ($p < 0.01$) compared to the control and only MNPs-loaded nanofiber mesh, which may benefit from CUR and can also cause HSP90-reduction [34]. A potential explanation for the effects of CUR on HSP90-related signaling pathways may be as an inhibitor of the Hsp90 heat shock protein [35]. This is consistent with the results on the role of CUR in inhibiting adenovirus replication by disruption of E1A protein *via* the Hsp90 dependant pathway [36,37] and the results on the role of CUR rescuing the nuclear localization and transactivation activity of mutated PHOX2B carrying the most significant expansion of polyAla in CCHS, where curcumin exerts an effect analogous to canonical Hsp90 inhibitors such as 17-AAG. In particular, the expression of HSP90 was markedly decreased in the MNPs/DOX/CUR@NFM group with AMF application compared to other groups ($p < 0.01$) despite the heating caused by the MNPs in the nanofiber, which facilitates HSP90 expression. These results suggested that CUR can enhance the anticancer efficiency of DOX in MCF-7/ADR cells *via* the reversion of drug resistance and Inhibition of HSP90 expression. This thermo-chemotherapy system could be an idealistic combination anticancer strategy for future cancer treatments.

3.8. Amplified anti-tumor efficacy by synergistic nanofiber mesh in vivo

Encouraged by the above results, an *in-vivo* anti-tumor efficacy was investigated using MCF-7/ADR carcinoma-bearing mice as a model to determine whether the thermo-chemotherapy nanofiber system would be effective in reducing tumor progression.

In order to evaluate the anticancer properties of nanofiber meshes, images of tumors obtained after three months are shown in Fig. 6 (A). As evident from the results, the tumors were reduced in size by DOX/CUR@NFM compared to free drug injection. Despite its initial efficacy, solution injection chemotherapy has a short half-life and rapid elimination. It was remarkable that MNPs/DOX/CUR@NFM + AMF were more effective than MNPs or drugs alone in reducing tumor size. Additionally, Fig. 6 (C) showed that the skin surface temperature transplanted with the MNPs-incorporated nanofiber mesh significantly increased from 27.7 °C to 39.1 °C under AMF for 15 min and showed time dependence (Fig. S2). Fig. 6 (B) shows that our proposed synergistic therapeutics of MNPs/DOX/CUR@NFM under AMF exposure achieved the most potent anti-tumor efficacy. It demonstrated a 92.9% inhibitory rate, proving the effectiveness of our synergistic strategy to improve anti-tumor outcomes.

Fig. 6 (E) shows that the tumor tissue therapied with MNPs/DOX/CUR@NFM under AMF application showed significantly decreased P-g protein expression compared to the control. It demonstrated that the group MNPs/DOX/CUR@NFM + AMF could efficiently inhibit the *in vivo* expression of P-g protein, which subsequently induces reverse drug resistance. This trend further demonstrated the functional role of CUR in reversing DOX resistance through P-g protein reduction following the results of cell uptake efficiency (Fig. 4).

As shown in Fig. 6 (F), the expression of HSP90 following therapy with MNPs@NFM + AMF was increased compared with the control. It is probably induced by the heating generated by hyperthermia. However, the MNPs/DOX/CUR@NFM + AMF groups showed a notable decrease in HSP90 expression compared to the MNPs@NFM + AMF group, which may benefit from DOX and can also cause HSP90-reduction. These trends are consistent with the results of Western blot analysis (Fig. 5). These results suggested that the combination therapy system (MNPs/DOX/CUR@NFM + AMF) can promote the anticancer efficiency of thermo-chemotherapy by reversing drug resistance and interfering with heat shock protein expression. This thermo-chemotherapy system could be an idealistic combination anticancer strategy for future cancer treatments.

3.9. Safety evaluation of nanofiber mesh

To evaluate the safety profiles and potential toxicities of the proposed thermo-chemotherapy nanofiber system by Liver biochemical indicators, H&E and masson trichrome staining. The safety assay was conducted after three months of treatment of MNPs/DOX/CUR@NFM transplanted into mice.

Given liver enzymes originating in the cell interior, the relatively elevated levels implied some liver damage [38]. As indicated in Fig. 6 (E), ALT and AST plasma levels post-treatment indicated negligible liver toxicities, given their comparability to those without any treatment.

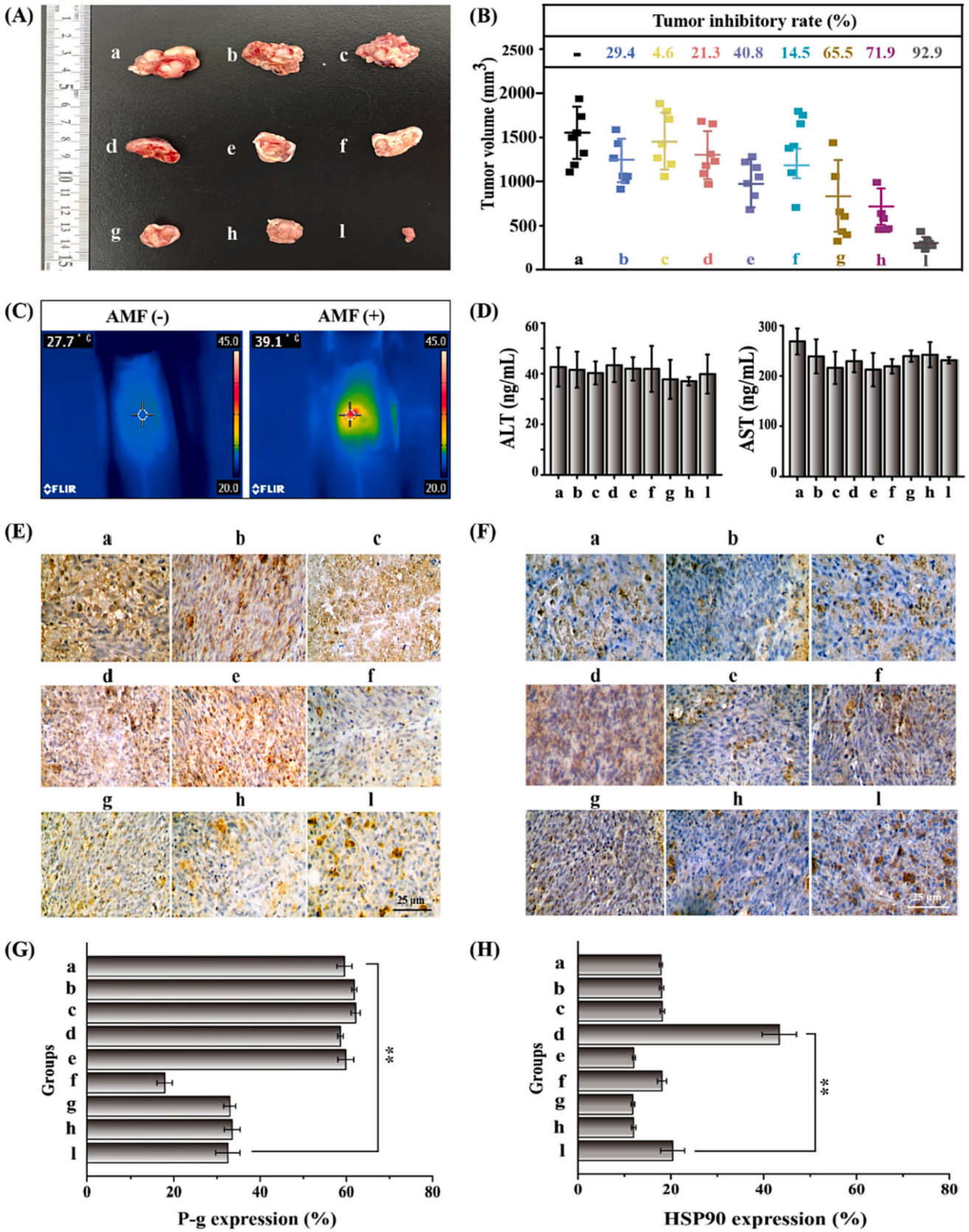

Fig. 6. (A) Tumor tissue volume images (B) Tumor volume after treatment of nanofiber and AMF exposure. (C) Infrared thermal images of mice transplanted with nanofiber mesh under 15 min of AMF irradiation. (D) Plasma ALT and AST levels in mice. Immunohistochemistry of P-g protein (E and G) and HSP90 protein (F and H) in tumor sections following therapy with nanofiber meshes. The intensity of protein expression was quantified using ImageJ software and the relative densitometries were summarized as bar graphs. (Mean ± S. D., $n = 3$; Student t-test, $^{**}p < 0.01$) (a: Control, b: Free drugs, c: PCL Blank NFM, d: MNPs@NFM + AMF, e: DOX@NFM + AMF, f: CUR@NFM + AMF; g: DOX/CUR@NFM + AMF; h: MNPs/DOX/CUR@NFM; l: MNPs/DOX/CUR@NFM + AMF).

As is well known, most chemotherapeutic agents have severe side effects, such as organ toxicity, compromising their therapeutic efficacy. In order to investigate nanofiber mesh safety further, the toxicities of the main organs were analyzed through H&E staining. In Figs. 7 (A) and S3, H&E staining was shown for the heart, lung, liver, spleen, and kidney. The tissues of these organs were not significantly damaged by MNPs/DOX/CUR@NFM groups under AMF exposure compared to the organs in the control group. Interestingly, in the final treatment group, compared with the control group, the tumor cells showed aggregations of variable-sized cobblestone cells with apoptotic nuclei separated by vascular congestion and vacuolations. Apoptosis was shown to be occurring in tumor cells.

In chronic inflammation, organization, and scarring, collagen fibers can appear with the development of pathological processes. However, these fibers are often difficult to distinguish from fibrin in H&*E*-stained sections. Therefore, the toxicities of the main organs were further analyzed through Masson trichrome staining to investigate the safety of nanofiber meshes. For Masson trichrome staining, collagen fibers are blue, muscle fibers are red, and nuclei are blue-black. From Fig. 7 (B) and Fig. S4, compared to Masson trichrome staining on the heart, lung, liver, spleen, and kidney in the control group, no marked collagen deposition was exhibited in the tissues of the organ treated with the MNPs/DOX/CUR@NFM + AMF groups. Moreover, the persistence and safety of nanofiber mesh were shown in Fig. S5. The appearance of mice skin and nanofiber mesh did not change significantly after the nanofiber mesh was implanted in the mice after three months. It may benefit from the good biocompatibility and slow degradation of PCL. These results demonstrate that no prominent systemic toxicities were indicated for our proposed thermo-chemotherapy nanofiber system (MNPs/DOX/CUR@NFM), a promising therapeutic system for future cancer therapy.

4. Conclusions

In the current research, we designed multifaceted thermo-chemotherapy nanofiber systems to simultaneously entrap and sustained release chemotherapy drugs of different physicochemical properties, as well as payload MNPs for mild heating, thereby reversing MDR and maximizing cancer cell sensitivity to thermo-chemotherapy. The nanofiber produced *via* electrospinning has a homogeneous distribution of MNPs and can provide controlled heating with an external AMF. The nanofiber mesh provided long-term antitumor efficacy by sustaining the release of DOX and CUR for two months. *In vitro* and *in vivo* studies demonstrated that nanofibers had superior antitumor effects over a single drug and heating alone. Consequently, these studies suggest that locally implantable thermotherapy nanofiber systems may provide an avenue for increasing the efficacy of current chemotherapy at reduced loadings in treating postoperative breast cancer.

Author contributions

Experimental design: Lili Chen and Mitsuhiro Ebara; experimental preparation: Lili Chen Ahmed Nabil and Kai Li; data analysis: Lili Chen; chart production: Lili Chen; writing-original draft preparation: Lili Chen; writing-review and editing: Lili Chen, Mitsuhiro Ebara, Ahmed Nabil, Nanami Fujisawa and Emiho Oe. All authors have read and agreed to the published version of the manuscript.

CRediT authorship contribution statement

Lili Chen: Visualization, Validation, Supervision, Software, Resources, Project administration, Methodology, Investigation, Formal analysis, Data curation, Conceptualization, Writing - original draft, Writing - review & editing. **Ahmed Nabil:** Investigation, Data curation. **Nanami Fujisawa:** Writing – original draft, Project administration. **Emiho Oe:** Project administration. **Kai Li:** Project administration, Data curation. **Mitsuhiro Ebara:** Visualization, Validation, Supervision, Software, Resources, Project administration, Methodology, Investigation, Funding acquisition, Formal analysis, Data curation,

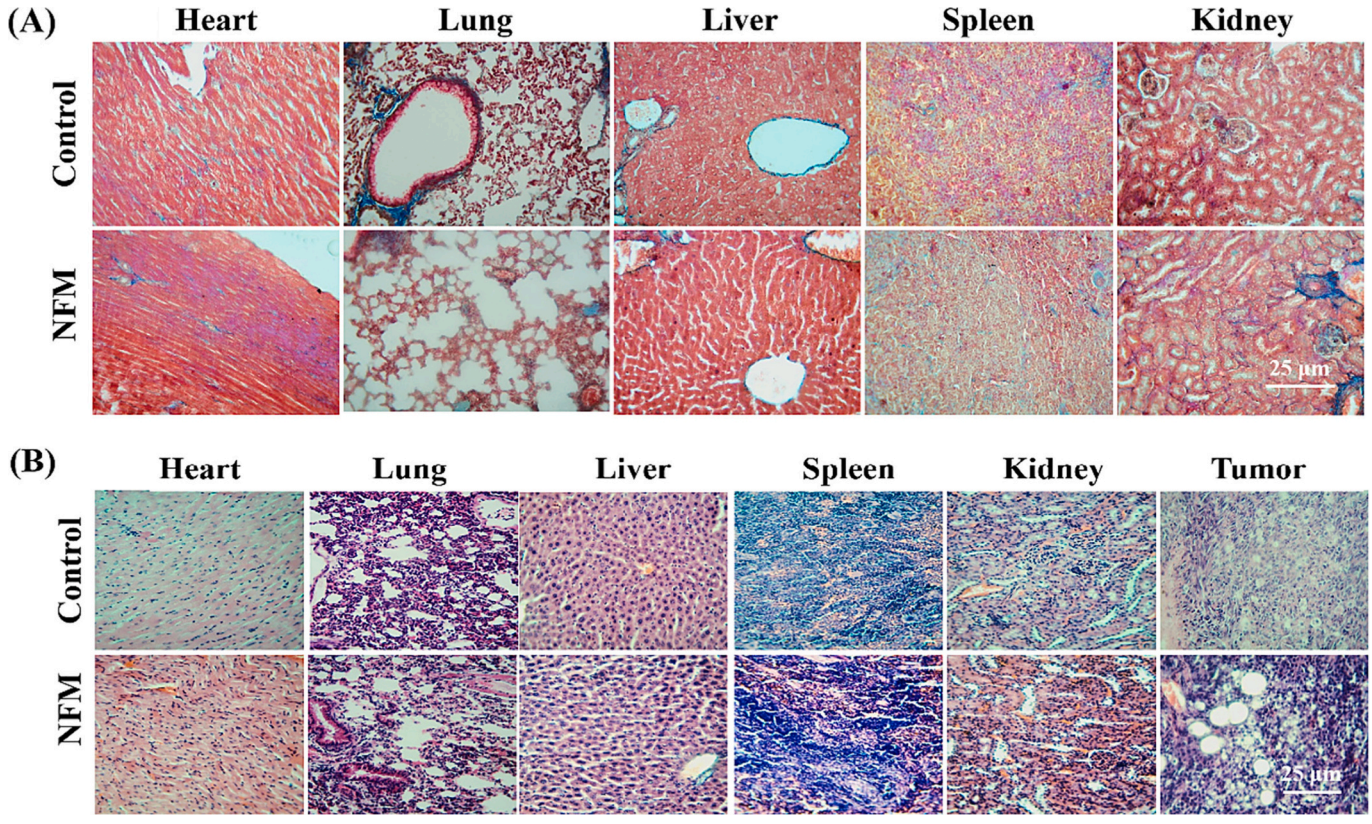

Fig. 7. Histologic assessments of major organs with (A) H&E staining and (B) Masson trichrome staining in MNPs/DOX/CUR@NFM + AMF treated mice.

Conceptualization, Writing - original draft, Writing - review & editing.

Declaration of Competing Interest

None.

Data availability

Data will be made available on request.

Acknowledgments

This study was supported by JSPS KAKENHI Grant-in-Aid for Scientific Research (B) (JP19H04476) and Grant-in-Aid for Transformative Research Areas (A) (JP20H05877).

Appendix A. Supplementary data

Supplementary data to this article can be found online at https://doi.org/10.1016/j.jconrel.2023.10.010.

References

[1] Y. Liang, H. Zhang, X. Song, Q. Yang, Metastatic heterogeneity of breast cancer: molecular mechanism and potential therapeutic targets, Semin. Cancer Biol. 60 (2020) 14–27.
[2] Y. Li, X. Xu, Nanomedicine solutions to intricate physiological-pathological barriers and molecular mechanisms of tumor multidrug resistance, J. Control. Release 323 (2020) 483–501.
[3] G. Zhong, C. Yang, S. Gao, N. Park, Y. Huang, M.H. Tan, X. Wang, J.L. Hedrick, W. Fan, Y.Y. Yang, Polymers with distinctive anticancer mechanism that kills MDR cancer cells and inhibits tumor metastasis, Biomaterials 199 (2019) 76–87.
[4] O. Tacar, P. Sriamornsak, C.R. Dass, Doxorubicin: an update on anticancer molecular action, toxicity and novel drug delivery systems, J. Pharm. Pharmacol. 65 (2013) 157–170.
[5] L. Wang, J. Yang, Q. Hou, S. Liu, X. Jiang, Mercaptophenylboronic acid-activated gold nanoparticles as nanoantibiotics against multidrug-resistant bacteria, ACS Appl. Mater. Interfaces 12 (2020) 51148–51159.
[6] H.H. Chen, I.L. Lu, H.C. Chiu, Indocyanine green/doxorubicin-encapsulated functionalized nanoparticles for effective combination therapy against human MDR breast cancer, Coll. Surf. B 177 (2019) 294–305.
[7] K. Ewon, A.S. Bhagya, A review on golden species of zingiberaceae family around the world: genus curcuma, Afr. J. Agric. Res. 14 (2019) 519–531.
[8] K. Yang, Z. Yang, G. Yu, Z. Nie, X. Chen, Polyprodrug nanomedicines: an emerging paradigm for cancer therapy, Adv. Mater. 34 (2021) 2107434–2107446.
[9] Y.J. Kim, M. Ebara, T. Aoyagi, A smart hyperthermia nanofiber with switchable drug release for inducing cancer apoptosis, Adv. Funct. Mater. 23 (2013) 5753–5761.
[10] D. Sakpal, S. Gharat, M. Momin, Recent advancements in polymeric nanofibers for ophthalmic drug delivery and ophthalmic tissue engineering, Biomater. Adv. 141 (2022) 213124–213138.
[11] A.T. Iacob, D. Lupascu, An overview of biopolymeric electrospun nanofibers based on polysaccharides for wound healing management, Pharmaceutics 12 (2020) 13–30.
[12] H.F. Rodrigues, A.F. Bakuzis, In vivo magnetic nanoparticle hyperthermia: a review on preclinical studies, low-field nano-heaters, noninvasive thermometry and computer simulations for treatment planning, Int. J. Hyperth. 37 (2020) 76–99.
[13] S.V. Spirou, A. Laurenzana, A.I. Barbosa, I.G. Alonso, C. Jones, D. Jankovic, O. L. Gobbo, Recommendations for in vitro and in vivo testing of magnetic nanoparticle hyperthermia combined with radiation therapy, Nanomaterials 8 (2018) 238–249.
[14] M.M. Paulides, D.B. Rodrigues, Recent technological advancements in radiofrequency- andmicrowave-mediated hyperthermia for enhancing drug delivery, Adv. Drug Deliv. Rev. 163-164 (2020) 3–18.
[15] K. Mortezaee, A. Narmani, M. Najafi, Synergic effects of nanoparticles-mediated hyperthermia in radiotherapy/chemotherapy of cancer, Life Sci. 269 (2021) 119020–119033.
[16] D.C. Phung, H.T. Nguyen, T.T. Phuong Tran, S.G. Jin, C.S. Yong, D.H. Truong, T. H. Tran, J.O. Kim, Combined hyperthermia and chemotherapy as a synergistic anticancer treatment, J. Pharm. Investig. 49 (2019) 519–526.
[17] K. Rajendran, U.M. Krishnan, Emerging trends in nano-bioactive-mediated mitochondria-targeted therapeutic stratagems using polysaccharides, proteins and lipidic carriers, Int. J. Biol. Macromol. 208 (2022) 627–641.
[18] L. Wang, C. Gao, X. Du, J. Zhou, Cypate-conjugated porous upconversion nanocomposites for programmed delivery of heat shock protein 70 small interfering RNA for gene silencing and photothermal ablation, Adv. Funct. Mater. 26 (2016) 3480–3489.
[19] S. Guo, L. Lv, Z. Hu, Q. He, A nanoparticulate pre-chemosensitizer for efficacious chemotherapy of multidrug resistant breast cancer, Sci. Rep. 6 (2016) 21459–21472.
[20] W. Li, B. Li, B. Wu, B. Tian, X. Chen, C. Wang, W. Hong, J. Peng, Free-radical cascade generated by aiph/Fe_3O_4-coloaded nanoparticles enhances mri-guided chemo/thermodynamic hypoxic tumor therapy, ACS Appl. Mater. Interfaces 14 (2022) 29563–29576.
[21] S. Nemec, S. Kralj, J.K. Tabi, Comparison of iron oxide nanoparticles in photothermia and magnetic hyperthermia: effects of clustering and silica encapsulation on nanoparticles' heating yield, Appl. Sci. 10 (2020) 7322–7337.
[22] L. Chen, F.L. Ji, Y.M. Bao, J. Xia, L. Guo, J.Y. Wang, Y.C. Li, Biocompatible cationic pullulan-g-desoxycholic acid-g-PEI micelles used to co-deliver drug and gene for cancer therapy, materials science & engineering, C, Mate. Biol. Applicat. 70 (2017) 418–429.
[23] C. Fu, L. Lin, H. Shi, S. Gao, X. Zhu, X. Chen, Hydrophobic poly (amino acid) modified PEI mediated delivery of rev-casp-3 for cancer therapy, Biomaterials 33 (2012) 4589–4596.
[24] D. Rong, P. Chen, Y. Yang, Q. Li, W. Wan, X. Fang, J. Zhang, Z. Han, J. Tian, J. Ouyang, Fabrication of gelatin/pcl electrospun fiber mat with bone powder and the study of its biocompatibility, J. Functi. Biomater. 7 (2016) 76–91.
[25] N. Maftoonazad, D. John, Development and evaluation of antibacterial electrospun pea protein isolate-polyvinyl alcohol nanocomposite mats incorporated with cinnamaldehyde, Mater. Sci. Eng. C 94 (2019) 393–402.
[26] Y.J. Kim, M. Ebara, T. Aoyagi, A smart nanofiber web that captures and releases cells, Angew. Chem. 51 (2012) 10537–10541.
[27] L. Azfarniam, M. Norouzi, Multifunctional polyester fabric using a multicomponent treatment, Fiber. Polym. 17 (2016) 298–304.
[28] K. Suzuki, H. Tanaka, M. Ebara, K. Uto, K. Okada, T. Murase, H. Yoshikawa, Electrospun nanofiber sheets incorporating methylcobalamin promote nerve regeneration and functional recovery in a rat sciatic nerve crush injury model, Acta Biomater. 53 (2017) 250–259.
[29] E.J. Furlani, E.P. Furlani, A model for predicting magnetic targeting of multifunctional particles in the microvasculature, J. Magn. Magn. Mater. 312 (2007) 187–193.
[30] P. Zhang, Y. Li, W. Tang, J. Zhao, L. Jing, K.J. McHugh, Theranostic nanoparticles with disease-specific administration strategies, Nano Today 42 (2022) 101335–101347.
[31] M. Li, W. Bu, X. Gao, P. Wang, Enhanced synergism of thermo-chemotherapy for liver cancer with magnetothermally responsive nanocarriers, Theranostics 8 (2018) 693–709.
[32] M. Norouzi, Z. Abdali, S. Liu, D.W. Miller, Salinomycin-loaded nanofibers for glioblastoma therapy, Sci. Rep. 8 (2018) 9377.
[33] S. Liu, Y. Yan, S. Pu, Y. Liang, Y. Zhao, Y. Zhang, J. Xie, Paclitaxel-loaded magnetic nanocrystals for tumor neovascular-targeted theranostics: an amplifying synergistic therapy combining magnetic hyperthermia with chemotherapy, Nanoscale 13 (2021) 3613–3626.
[34] U. Sarangi, J.U. Kumar, A.S. Sreedhar, 17AAG treatment accelerates doxorubicin induced cellular senescence: Hsp90 interferes with enforced senescence of tumor cells, Drug Target Insight. 6 (2012) 19–39.
[35] A.A. Ahmed Abdelmoaty, P. Zhang, W. Lin, Y.J. Fan, S.N. Ye, J.H. Xu, C0818, a novel curcumin derivative, induces ROS-dependent cytotoxicity in human hepatocellular carcinoma cells in vitro via disruption of Hsp90 function, Acta Pharmacol. Sin. 2 (2022) 446–456.
[36] I. Dalidowska, O. Gazi, D. Sulejczak, M. Przybylski, P. Bieganowski, Heat shock protein 90 chaperones E1A early protein of adenovirus 5 and is essential for replication of the virus, Int. J. Mol. Sci. 4 (2021) 2020–2035.
[37] M.R. Jennings, J.P. Robin, Antiviral effects of curcumin on adenovirus replication, Microorganisms 10 (2020) 1524–1540.
[38] H.Y. Cui, L.L. Chen, M. Qian, X. Zheng, X. Yang, L. Chen, Y. Zhao, Q.X. Chen, J. Y. Wang, Chemotherapeutic potency stimulated by SNAI1-knockdown based on multifaceted nanomedicine, J. Control. Release 337 (2021) 343–355.